PCCP

ROYAL SOCIETY OF CHEMISTRY

PAPER

View Article Online
View Journal | View Issue

Cite this: *Phys. Chem. Chem. Phys.*, 2024, **26**, 29788

Developing a biosensing prototype utilising a 7CB liquid crystal for human insulin detection†

Athul Satya and Ayon Bhattacharjee *

This paper presents a novel prototype for human insulin detection using a 4-heptyl-4-biphenyl-carbonitrile liquid crystal (7CB-LC). Human insulin is essential for regulating blood glucose levels and facilitating the metabolism of carbohydrates, lipids, and proteins. Insufficient insulin can lead to hyperglycemia, where cells cannot utilise glucose effectively for energy production. Prolonged hyperglycemia can affect the nervous and cardiovascular systems. Our work investigates the scope of using 7CB-LC as a prototype for the label-free detection of human insulin. Both temperature and time-dependent studies conducted using a polarising optical microscope (POM) on human insulin in the concentration range from 25 μM to 500 μM showed that human insulin interacting with 7CB-LC produces radial, twisted-radial, pre-radial and bipolar textures. A detection limit of 25 μM was observed since no distinguishable textures were observed below this concentration. An RGB (red, green, and blue) and grey index study showed a positive correlation graph with an R^2 value of 0.97279, proving the selectivity of the proposed biosensor. Molecular docking and Raman spectroscopy studies were conducted to learn more about the interaction between insulin and 7CB-LC at the molecular level. Docking studies revealed how the position of the 7CB core and tail ends interacted with amino acid residues of insulin. Raman spectroscopy studies investigated the segmental mobility of different parts of LC and changes occurring in the core and terminal regions due to insulin interactions. Vibrational studies conducted using Raman spectroscopy analysed the change in 7CB-LC parameters such as the peak position (PP), line width (LW) and integrated intensity (II) on interacting with human insulin. This unique prototype technique shows how 7CB-LC can potentially be employed in biosensing to detect human insulin since it provides better visualisation in a label-free detection method.

Received 14th August 2024,
Accepted 15th November 2024

DOI: 10.1039/d4cp03205e

rsc.li/pccp

1. Introduction

Liquid crystals (LCs) are a specific state of matter that are anisotropic and exhibit the properties of both solids and liquids.[1] Based on the transition mode to mesophases, LCs can be classified into thermotropic LCs and lyotropic LCs. LCs, as biosensors, were developed for the first time by Abbot *et al.* in 1998 to detect anti-Bi-IgG (anti-bispecific immunoglobin G) and avidin.[2] Our work investigates the scope of using a 4-heptyl-4-biphenylcarbonitrile (7CB) LC for the label-free detection of human insulin. Human insulin is a peptide hormone synthesised by pancreatic beta cells within the islets of Langerhans. It is integral in maintaining blood glucose levels and overseeing the metabolism of carbohydrates, lipids, and proteins.[3] It facilitates cell division and growth by exerting mitogenic influences. Human insulin shortage can cause various health issues, mostly due to the cell's inability to use glucose as an energy source. This can cause hyperglycemia, which can develop into diabetes mellitus and affect the nervous and cardiovascular systems.[3,4]

Traditional insulin detection methods include enzyme-linked immunosorbent assay (ELISA), fully automated immunoassay platforms and chromatography techniques. In addition to these, tests such as the arginine simulation test and hyperglycemic clamp test help in evaluating insulin secretion in the human body. These methods require complicated instrumentation techniques, are time-consuming, and are costly for the day-to-day insulin monitoring.[5] An aptamer-based biosensor was developed for insulin detection by Yoshida *et al.* in 2009, employing a process known as SELEX (systematic evolution of a ligand by exponential enrichment). In this process, DNA aptamers were isolated against insulin to select IGA3 (insulin growth aptamer) because of its high affinity towards insulin. IGA3 was later used in an enzyme system with a thrombin-inhibiting aptamer, which releases thrombin when insulin binds.[6] In 2020, Piletsky *et al.* developed a molecular imprinting (MIP) based insulin biosensor

Department of Physics, National Institute of Technology, Bijni Complex, Laitumkhrah, Shillong, Meghalaya 793003, India. E-mail: ayonbh@nitm.ac.in; Tel: +91 9485177033

† Electronic supplementary information (ESI) available. See DOI: https://doi.org/10.1039/d4cp03205e

using insulin MIP nanoparticles, immobilising them on a screen-printed electrode made of platinum for insulin detection.[7]

In efforts to reduce the costs associated with producing insulin detection methods, label-free detection techniques were developed. Notably, LC label-free detectors emerged as significant advancements, as they streamline electronics by employing LCs as electrochemical or optical transducers. In 2023, Servarayan *et al.* introduced a label-free fluorescence-based biosensor for insulin detection in human serum, employing naturally occurring chromene mimic receptors.[8] Label-free detection of insulin using a LC was introduced by Chen and colleagues, developing a label-free aptamer-based optical LC biosensor for insulin detection using a 4-cyano-4-pentyl biphenyl (5CB) LC. This biosensor utilised an aptamer (IGA3) adsorbed to cetyltrimethylammonium bromide (CTAB) and detected insulin-induced conformational changes at the aqueous–liquid crystal interface using polarised optical microscopy (POM).[9] All these detection techniques, besides being label-free, used aptamers and other chemical reagents to attain selectivity and high sensitivity. Besides the positive correlation observed between grey scale analysis and concentration, the ability of Chen *et al.*'s biosensor to accurately quantify insulin remains limited. Conversely, our biosensor model demonstrates a quantitative detection method using less chemical reagents and responds to both time and temperature parameters, showing improved potential for precise sample analysis.

Our research explores the potential of detecting human insulin utilising 7CB-LC without aptamers. Currently, there are no biosensors utilising 7CB-LC for label-free detection of insulin. Optical studies conducted using POM showed that 7CB-LC on interacting with human insulin produces schlieren textures having radial, twisted-radial, pre-radial and bipolar textures. Both time and temperature studies were conducted to know the appropriate temperature for the developed biosensor. Concentrations of insulin ranging from 25 μM to 500 μM were studied. The temperature studies show that temperatures ranging from 22 °C to 40 °C are the most appropriate for the proposed biosensor. The quantitative analysis measured the greyscale intensity (GI) values of the POM images, and a correlation graph was plotted between the insulin concentrations and GI values. The correlation graph showed a positive correlation, having an R^2 value of 0.97279. The prototype biosensor demonstrated a detection limit of 25 μM, as distinguishable textures were not observed below this concentration.

To learn more about the interaction between insulin and 7CB-LC at the molecular level, molecular docking studies using auto dock tools and vibrational studies using Raman spectroscopy were conducted. The docking studies showed that amino acid residues such as leucine (Leu) 15, arginine (Arg) 22, phenylalanine (Phe) 24, 25 and tyrosine (Tyr) 26 present in human insulin were found to form hydrophobic interactions with 7CB-LC. Samples were analysed within a range of 1000–3200 cm^{-1} using Raman spectroscopy, and six significant peaks were observed at wavelengths 1180 cm^{-1}, 1287 cm^{-1}, 1525 cm^{-1}, 1608 cm^{-1}, 2223 cm^{-1} and 2848 cm^{-1}. Vibrational analyses revealed that interaction between 7CB and human insulin induces a notable symmetric–asymmetric stretch in the (C–H) aliphatic chains and (C–C) aromatic rings of 7CB-LC, particularly in the presence of the phenylalanine (Phe) amino acid residue found in insulin. The overall studies show the possibility of developing a label-free biosensor using 7CB-LC to detect human insulin. Despite the average human insulin concentration in the body being 90 pmol L^{-1}, our biosensor serves as a pioneering prototype model for utilising 7CB-LC in detecting human insulin.

2. Methodology

2.1 Materials

Sigma Aldrich provided the key raw materials, which included human insulin, 4-heptyl-4-biphenylcarbonitrile (7CB), and dimethyl octadecyl [3-(trimethoxysilyl)propyl] ammonium chloride (DMOAP). The materials were used without any purification. Insulin solutions at various concentrations were prepared using phosphate-buffered saline (PBS) with a buffer strength of 20 mM and a pH of 7.4. The insulin molar extinction coefficient (ε_{molar}) was 5734 M^{-1} cm^{-1} at 280 nm, measured with a UV-Vis spectrophotometer (Shimadzu UVPC 2450 Corporation, Tokyo, Japan). Fig. 1(a) depicts the molecular structure of human insulin: chains A and B. Chain A comprises 21 amino acids, whereas chain B has 30 amino acids. The chemical structure of 7CB is shown in Fig. 1(b).

2.2 Method of preparation of a DMOAP-coated glass slide

1% (v/v) DMOAP solution was prepared by mixing 1 mL of DMOAP with 100 mL of deionised water. Glass slides were cleaned using a solution of ethanol and deionised water, followed by ultrasonication and baking at 80 °C for 15 minutes. After cleaning, the glass slides were immersed in the DMOAP solution for 15 minutes and then baked again for another 15 minutes. This process resulted in DMOAP-coated glass slides that facilitate the homeotropic alignment of the liquid crystal.

2.3 Method of preparation of insulin-7CB cell

To construct 7CB-insulin cells, glass slides were coated with DMOAP solution. 0.5 μL of 7CB-LC was added above the DMOAP-coated glass slide. A Myler spacer with a square inlet was kept above the DMOAP-coated glass slide, which acted as a spacer. Later, the same volume of insulin was introduced above the LC droplet using a micropipette. The resulting insulin-7CB droplet was let to settle for a few seconds. Later, the sample was sealed with a coverslip to create LC-insulin cells, as illustrated in Fig. 2. The cells were made with concentrations ranging from 25 μM to 500 μM. A cover slip was employed to maintain the stability of textures for a significant duration. Normal cover slips lacking the DMOAP coating were chosen to prevent double twisting in the arrangement of LC molecules, which could disrupt homeotropic alignment. Coverslips were specifically used to preserve texture stability on pre-coated glass slides.

2.4 Characterisation techniques

2.4.1. Polarising optical microscopy studies. Polarising optical microscopy (POM) is a common microscopic technique

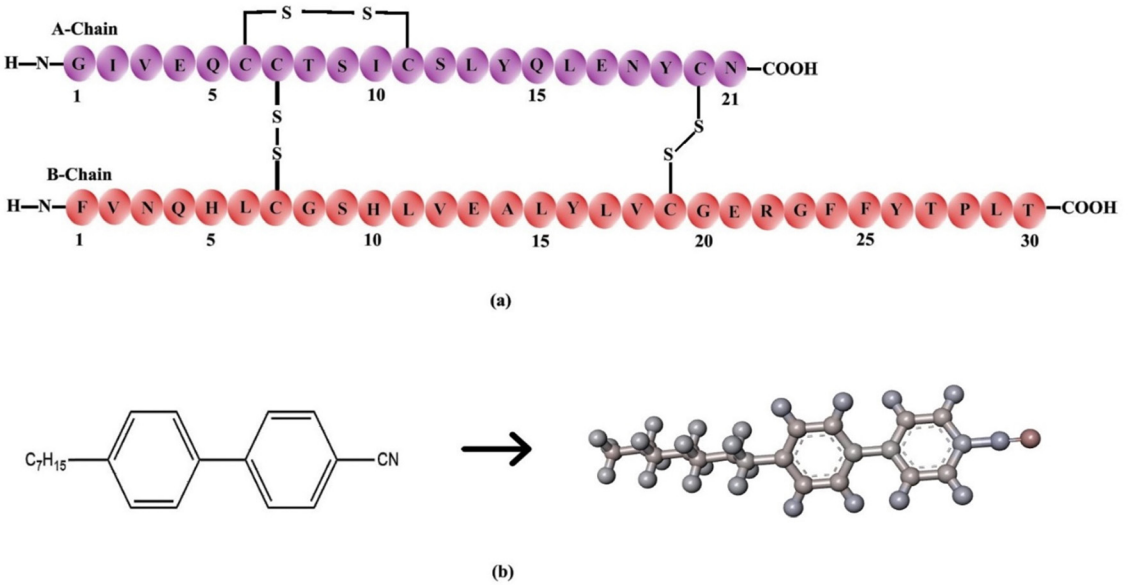

Fig. 1 (a) Primary structure of insulin showing the amino acid sequence of chain A and chain B, (b) chemical structure of the 4-heptyl-4-biphenylcarbonitrile (7CB) liquid crystal.

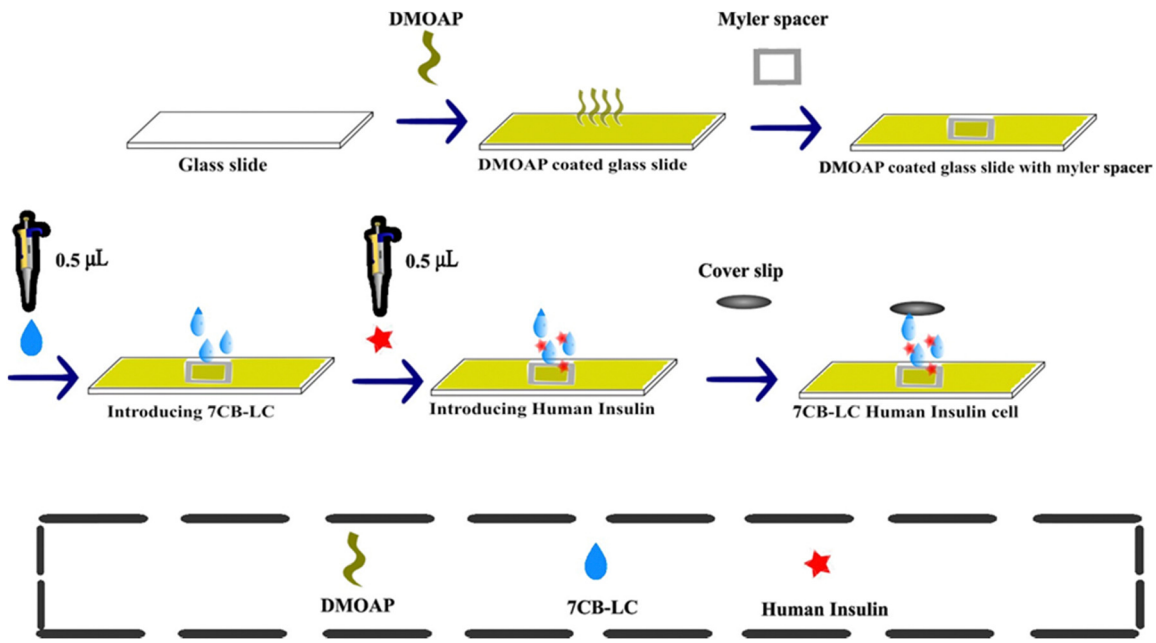

Fig. 2 Preparation of 7CB-insulin cell.

for studying materials such as LCs. POM uses polarised light to enhance and reveal specific properties of LCs, such as birefringence and anisotropy. It helps visualise the phase transitions and the corresponding textures. LC can undergo phase transitions such as the crystalline phase, smectic phase, nematic phase, and isotropic phase. A Leica DM2700P (Germany) POM was used in our optical studies. The LC-insulin cell was placed within a hot stage (Linkam LTS420, UK) attached to the POM, with the temperature controller linked to the hot stage to regulate a room temperature of 20 °C. Concentrations ranging from 25 µM to 500 µM were studied using the POM. In the POM setup, crossed polarisers were employed to examine the material. Rotating the stage 360 degrees and observing no transmitted light in the isotropic state revealed the optical isotropy of the LC sample or the absence of birefringence. Optical images were recorded using a Leica (MC170 HD) camera mounted on a microscope. Objectives having magnifications of 10×, 20×, and 50× were used for good resolution of the pictures.

2.4.2. Molecular docking studies. Molecular docking (MD) is a computational approach in structural molecular science

and computer-assisted drug design. It predicts the binding modes of a ligand to a protein of a known three-dimensional structure and the optimal orientation, affinity, and interactions between a ligand and a protein. This technique helps in drug design by analysing molecular interactions.[10] The 3D structure of human insulin was obtained from the protein data bank (**https://www.rcsb.org/**) using the PDB format ID 4EYN. The 7CB liquid crystal, which serves as the ligand, was retrieved in the SVG format from PubChem (**https://pubchem.ncbi.nlm.nih.gov/**), PubChem CID: 170468. The ligand is flexible in molecular docking, while the protein is rigid. The data log (DLG) file was created using Auto Dock Tool 1.5.7, containing details such as binding energy for various docked positions, lowest binding energy, mean binding energy, and root mean square difference (RMSD). Discovery Studio Visualizer 2021 was utilised for visualisation, while additional docking software programs like protein–ligand interaction profiler (PLP) and Lingplot+ V.2.2 were employed for extracting the molecular docking data.

2.4.3. Raman spectroscopy studies. Vibrational studies of 7CB-LC interacting with human insulin were conducted using Raman spectroscopy. The spectra were recorded using an inVia Raman spectrometer from Renishaw (UK), equipped with 532 nm lasers and a cooled charge coupled device detector. Concentrations ranging from 25 μM to 500 μM were analysed. The samples were kept in a dispersed glass slide coated with DMOAP. A Leica DM2700M microscope attached to the spectrometer having a magnification of a 20× long-distance object was used for the study. The system was calibrated by recording the spectra at 520 cm^{-1} using a silicon reference. The samples were analysed within a range of 1000–3200 cm^{-1}. The samples underwent analysis with a 20-second exposure time and a 5 mW laser power. Wire 5.5 software was employed for data extraction, and the collected data were processed using GRAMS software. Parameters such as peak position (PP), line width (LW), and integrated intensity (II) were determined following deconvolution using Lorentzian fitting.

3. Results and discussion

3.1 POM study of the 7CB-insulin interacting texture

3.1.1. Preparation of control parameters. Control parameters serve as a reference point or baseline against which experimental circumstances can be compared. It demonstrates the consistency and accuracy of the experimental methodology. 7CB-LC on a standard glass slide and 7CB-LC on a DMOAP-coated glass slide were used as the control parameters. DMOAP is hydrophobic in nature. It contains a quaternary ammonium group attached to an aliphatic octadecyl chain ($C_{26}H_{58}NO_3SiCl$). The long alkyl chain in DMOAP is responsible for its hydrophobicity and regulates its interactions with surfaces. It helps generate a homeotropic arrangement for the LCs.[11,12]

(a) 7CB-LC in a normal glass slide. The optical texture of 7CB-LC in a standard glass slide was studied using POM. A hexagonal texture was observed, as shown in Fig. 3(a).

(b) 7CB-LC interacting with human insulin on a normal glass slide. 7CB-LC, while interacting with human insulin on a normal glass slide, does not show any specific textures as shown in Fig. 3(b). Since the glass slides were not coated with DMOAP, LCs were poorly aligned, resulting in fewer interactions with human insulin.

(c) 7CB-LC on a DMOAP-coated glass slide. 7CB-LC on a normal glass slide shows a lamellar texture under the POM, as shown in Fig. 3(c).

(d) 7CB-LC interacting with human insulin on a DMOAP-coated glass slide. The homeotropic arrangement of 7CB-LCs generated by the DMOAP coating gives a better alignment for the LCs. 7CB-LC interacting with human insulin in a DMOAP-coated glass slide generated a twisted radial texture with four schlieren brushes and a point defect at the centre, as shown in Fig. 3(d).

3.1.2. Time and concentration study of the 7CB-insulin complex. A time study of 7CB-LC interacting with human insulin was conducted to study the variation of 7CB-LC under interaction with different insulin concentrations with respect to time. 7CB-LC, on interacting with insulin, creates director orientations in radial, twisted radial, pre-radial and bipolar textures, as shown in Fig. 4.[13] Concentrations such as 25 μM, 50 μM, 100 μM, 200 μM, 300 μM, 400 μM and 500 μM were studied for six hours, as shown in Fig. 5.

The POM analysis of blank cells shows that 7CB on a DMOAP-coated glass slide shows a lamellar texture, as shown in Fig. 5(a).

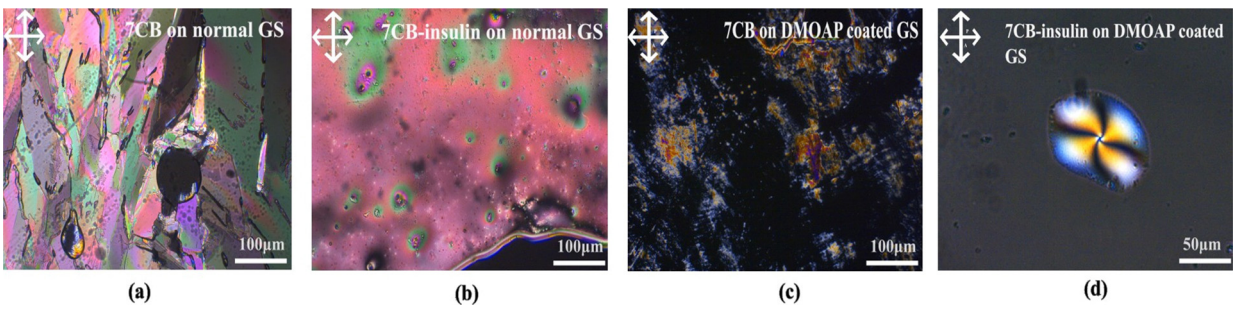

Fig. 3 (a) 7CB-LC observed on a glass slide, (b) interaction between insulin and 7CB-LC on a glass slide, (c) 7CB-LC observed on a glass slide coated with DMOAP, and (d) formation of a twisted radial texture with 7CB-insulin on a DMOAP-coated glass slide.

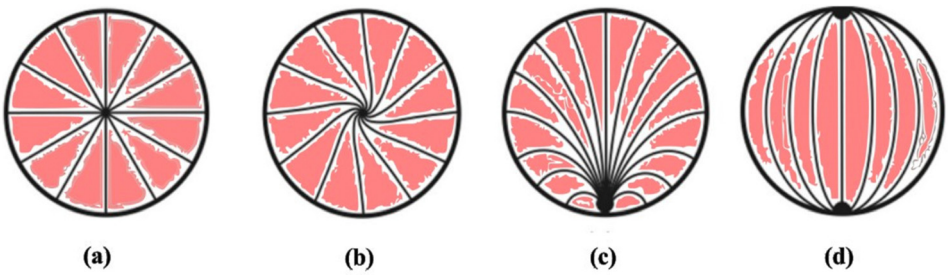

Fig. 4 Schematic representation of various kinds of director configurations observed in liquid crystal droplets in the nematic state: (a) radial having a point defect at the centre, (b) twisted radial having a point defect at the centre, (c) pre-radial having a point defect at the corner end and (d) bipolar having two-point defects at the corner ends.

At a concentration of 25 μM, no discernible textures were observed initially (0 minutes). However, after 30 minutes, a radial texture with four Schlieren brushes and a point defect at the centre was detected, as depicted in Fig. 5(b-ii). This radial texture persisted until 60 minutes, after which it disappeared. On increasing the concentration to 50 μM, thread-like textures were observed within 0 minutes. After 30 minutes, a twisted radial texture featuring four schlieren textures with a central point defect was detected, as illustrated in Fig. 5(c-ii). This twisted radial texture persisted until 180 minutes, as depicted in Fig. 5(c-iii–iv), before disappearing after 6 hours. Similar to the observation at a concentration of 25 μM, a radial texture was observed at a concentration of 100 μM, as depicted in Fig. 5(d).

At both 200 μM and 400 μM concentrations of insulin interacting with 7CB-LC, as shown in Fig. 5(e) and (g), a twisted radial texture was observed till 180 minutes. At a concentration of 300 μM insulin, a twisted radial texture was observed at 30 minutes, as illustrated in Fig. 5(f-ii). Subsequently, this radial texture transformed into a pre-radial texture characterised by four Schlieren brushes and a point defect at the top corner, as depicted in Fig. 5(f-iii). Similar to 100 μM concentration, a radial texture was observed in the case of 500 μM insulin concentration, as shown in Fig. 5(h).

Three main types of director orientations, such as radial, twisted radial and pre-radial textures, were observed for insulin concentrations between 25 μM and 500 μM. It was seen that, for both 200 μM and 500 μM concentrations of insulin, radial schlieren textures started to appear instantly within 0 minutes. At concentrations exceeding 500 μM, distinct liquid crystalline textures were not observed. Increased protein concentration results in protein crowding or aggregation within the protein structure. This aggregation causes steric hindrance, reducing the protein's interaction with LC molecules. Investigating the interactions between liquid crystals and various protein concentrations is essential for enhancing the sensitivity of detection techniques. This understanding plays a pivotal role in characterising the nature and strength of protein–liquid crystal interactions, which is valuable for developing biosensors and gaining insights into biological mechanisms.[14,15]

3.1.3. Temperature and concentration study of the 7CB-insulin complex. Temperature studies of the 7CB-human insulin complex of different concentrations ranging from 200 μM to 500 μM were conducted in a limited range of temperature between 22 °C to 40 °C where the LC remains in the nematic state as shown in Fig. 6. To conduct the temperature study; the 7CB-insulin cells were placed inside a hot stage connected to the POM. The experiments included heating at 3 °C per minute using a hot stage and decreasing the heating rate to 0.5 °C near transition points. No significant change in the textures was observed below 200 μM concentration.

At a concentration of 200 μM insulin, interaction with 7CB-LC at 22 °C results in a twisted radial texture characterised by four schlieren brushes and a central point defect, as depicted in Fig. 6(a-i). Upon raising the temperature to 27 °C, this twisted radial texture transitions into a radial texture, as shown in Fig. 6(a-ii). At temperatures around 30 °C and above, a bipolar texture is observed, as illustrated in Fig. 6(a-iii). On increasing the insulin concentration to 300 μM, concentric textures were observed till 30 °C, as shown in Fig. 6(b-i and ii). By 37 °C and above, these concentric textures were converted into a twisted radial texture, as shown in Fig. 6(b-iii–iv). In the case of 400 μM concentration of insulin, a pre-radial texture having four schlieren brushes and a point defect at the top corner was observed, as shown in Fig. 6(c-i). Increasing the temperature above 27 °C, this pre-radial texture was converted to a twisted radial texture, as shown in Fig. 6(c-ii–iii). For a concentration of 500 μM, a twisted radial texture with four schlieren brushes persisted until reaching 30.8 °C, as illustrated in Fig. 6(d-ii). As the temperature increased to 38.5 °C, the twisted radial textures began transitioning into a bipolar texture, and at 40 °C, a bipolar texture was fully observed, as depicted in Fig. 6(d-iv).

The investigation of temperature dynamics in LC-protein complexes assists in finding the appropriate temperature range for sensor performance and identifying temperature-sensitive regions important for certain biomolecular interactions. This insight increases biosensor sensitivity and selectivity, allowing for developing temperature-responsive biosensors capable of precisely and efficiently detecting and quantifying target molecules.

3.1.4. Selectivity, reproducibility and the detection limit. To verify the specificity of this method, the optical signals read out from other similar kinds of samples were evaluated under the same experimental conditions. Protein samples such as

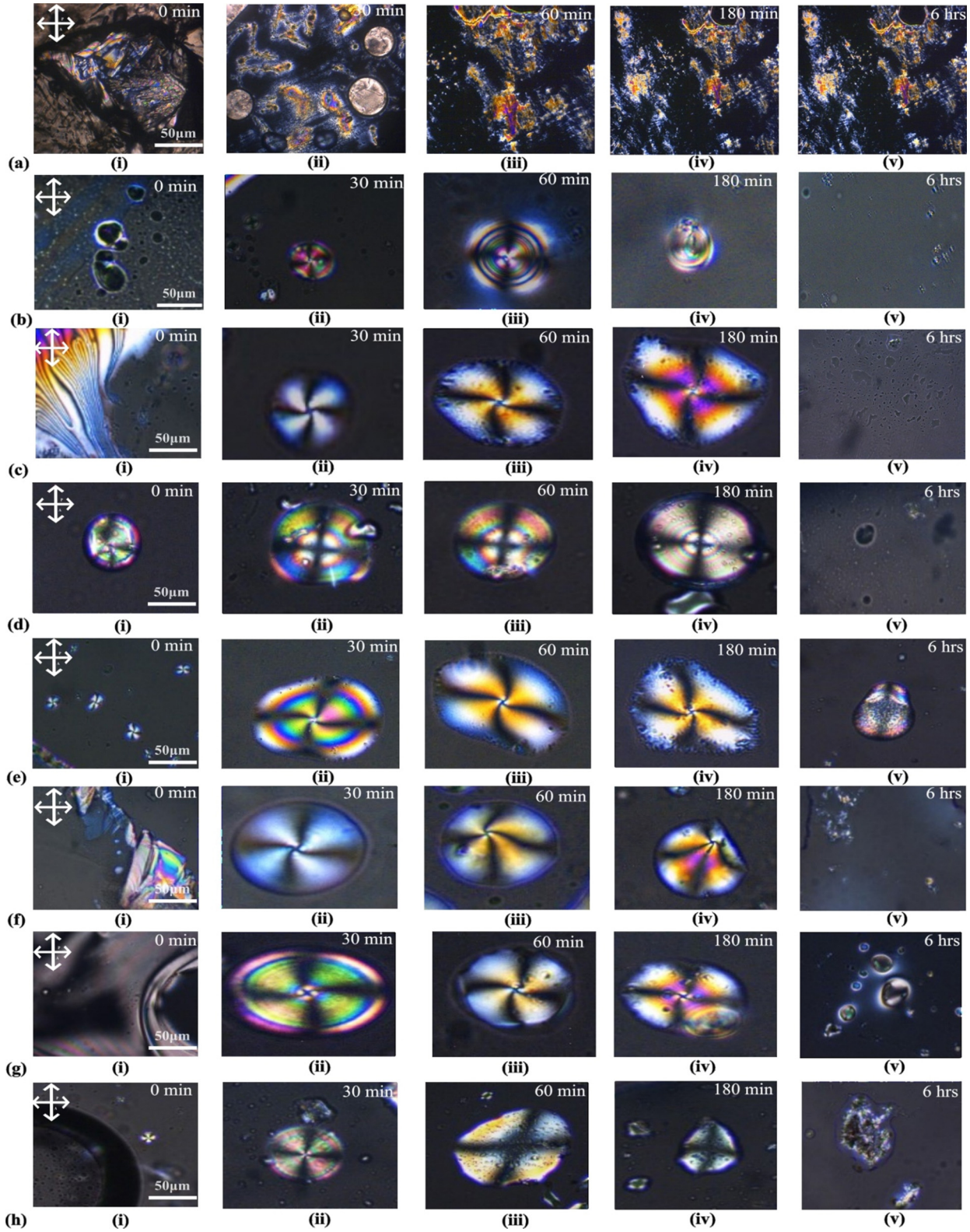

Fig. 5 Various morphological textures arising from the interaction between 7CB and insulin at different concentrations: (a) 7CB alone (blank sample), (b) 25 μM insulin, (c) 50 μM insulin, (d) 100 μM insulin, (e) 200 μM insulin, (f) 300 μM insulin, (g) 400 μM insulin, and (h) 500 μM insulin.

ascorbic acid, human serum albumin (HSA), human insulin, and a mixture of ascorbic acid, HSA, and human insulin interacting with 7CB-LC were evaluated. To ensure the accuracy of this study, all samples were standardised to 50 μM concentration and 0.5 μL

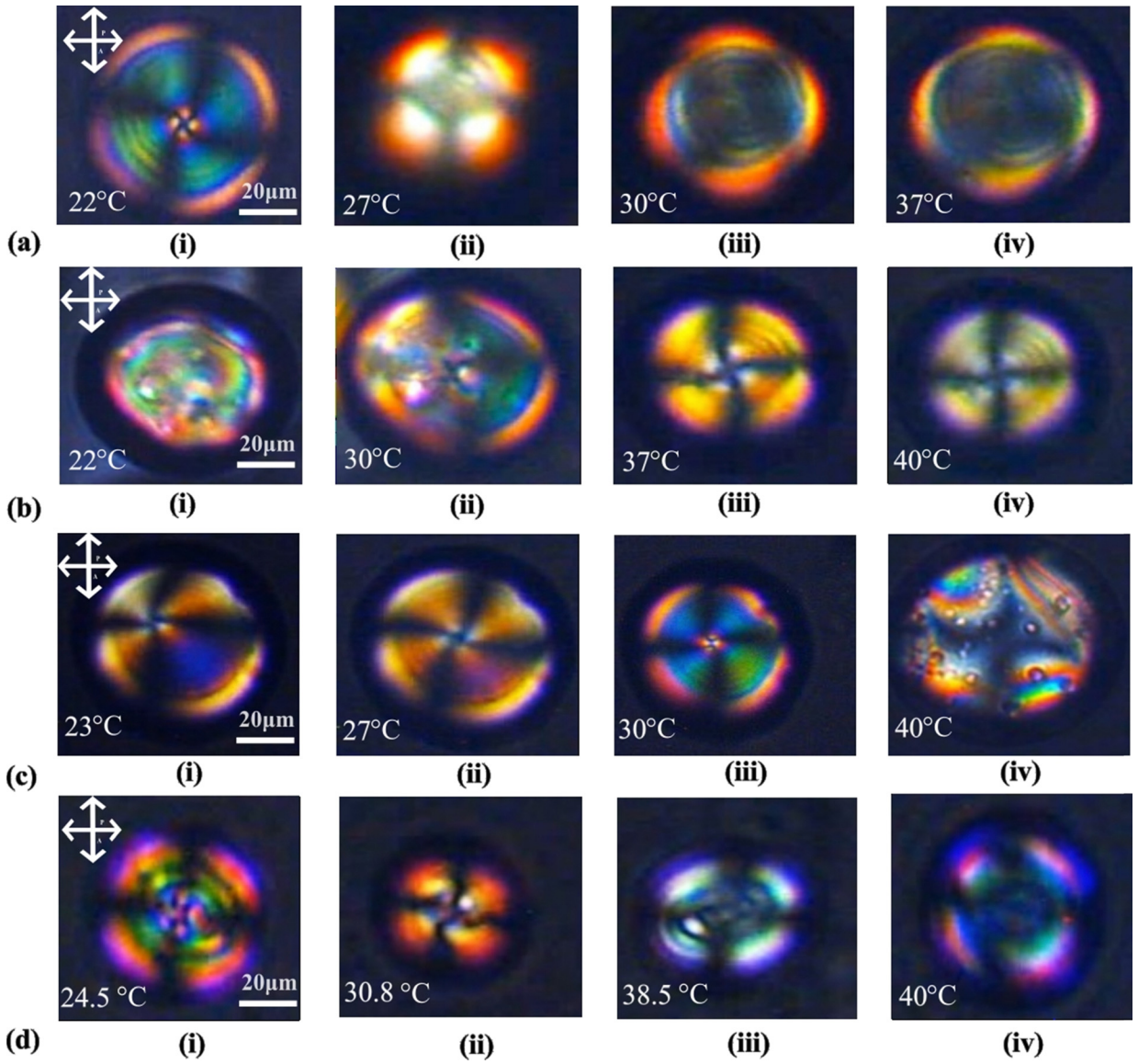

Fig. 6 POM images depicting temperature-induced changes in the morphological textures of the 7CB-insulin complex at various concentrations (a), 7CB interacting with 200 μM concentration of insulin, (b) 7CB interacting with 300 μM concentration of insulin, (c) 7CB interacting with 400 μM concentration of insulin and (d) 7CB interacting with 500 μM concentration of insulin.

volume. Ascorbic acid interacting with 7CB-LC has no significant selectivity, as shown in Fig. 7(a). In the case of HSA interacting with 7CB-LC, no specific Schlieren brushes were observed, as illustrated in Fig. 7(b). Whereas in the cases of 7CB-LC interacting with human insulin and 7CB-LC interacting with the ascorbic acid–HSA–insulin mixture, monochromatic optical textures were observed.

In both cases, a twisted radial texture having four Schlieren brushes and a point defect at the centre was observed, as shown in Fig. 7(c) and (d). To have a more scientific point of view, the RGB (red, green, blue) percentage values were measured as shown in Fig. 7. The RGB percentage values of POM images indicate that the more equal the distribution of RGB values is, the more successful the proteins disrupt the LC molecules. Fig. 7 shows that the RGB values are more equal in the case of insulin interacting with 7CB-LC.[16] These results show that human insulin shows enough selectivity towards 7CB-LC. Due to insufficient facilities for disposing of biohazards, our experiments were restricted to commercial samples.

POM observations indicate that no discernible textures were evident when human insulin interacts with 7CB-LC at concentrations below 25 μM. This implies that concentrations below 25 μM do not disturb the organised molecular arrangement of the LC. Therefore, the proposed prototype biosensor is observed to have a detection limit of 25 μM.

The concentrations were tested three times under the same experimental conditions, yielding comparable optical images and thus demonstrating partial reproducibility in the recorded results. Multiple measurements (3 times) were taken using ImageJ software to calculate the average grey-scale intensity

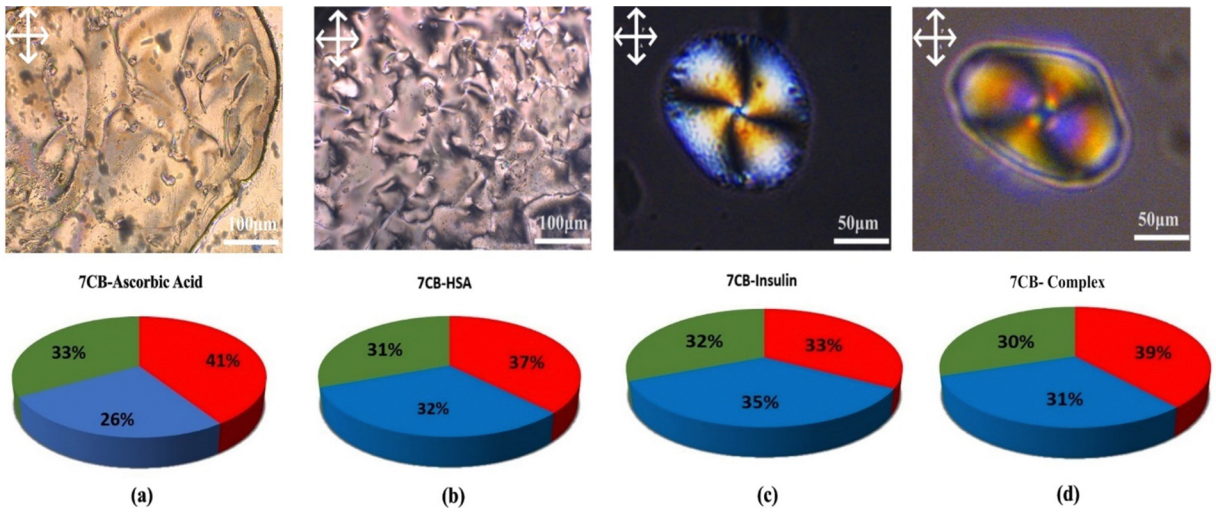

Fig. 7 POM images showing (a) the interaction between 7CB-LC and ascorbic acid, (b) the interaction between 7CB-LC and HSA forming a schlieren texture, (c) human insulin interacting with 7CB-LC forming a twisted radial texture, and (d) the interaction of a protein mixture (ascorbic acid, HSA and insulin) with 7CB-LC forming a twisted radial texture, along with their respective RGB values.

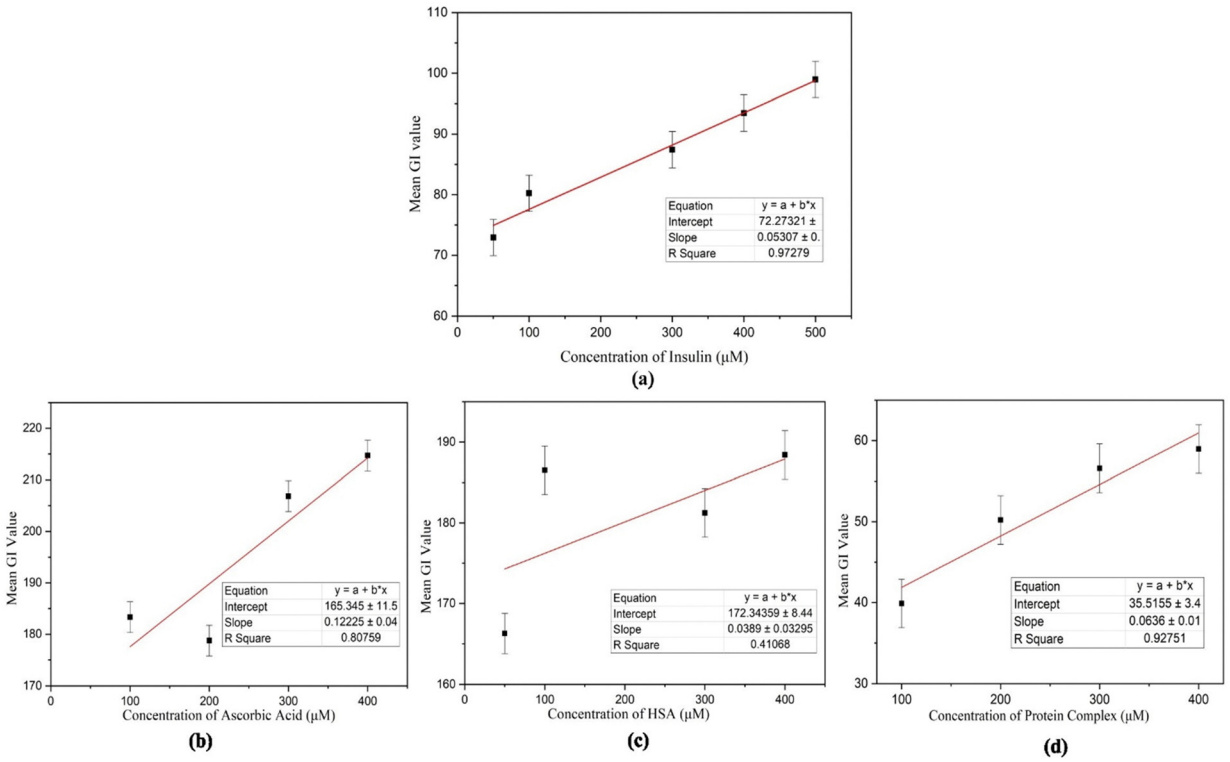

Fig. 8 (a) The calibration curve for HI demonstrates a strong positive correlation between insulin concentrations and its mean grayscale (GI) values, with an R^2 value of 0.97279, (b) for ascorbic acid, the calibration curve shows an R^2 value of 0.80759, (c) the calibration curve for HSA presents an R^2 value of 0.41068, and (d) the calibration curve for the protein mixture reveals an R^2 value of 0.92751.

(GI) within POM pictures to quantify the performance of the LC biosensor. Fig. 8 illustrates the calibration curve, which displays the average GI *versus* insulin concentration values ranging from 50 μM to 500 μM. This association was linear over the wide concentration range, with a significant correlation value (R^2) of 0.97279.

To confirm the specificity of human insulin detection, an interference study was conducted by analyzing the interactions of other proteins with 7CB-LC. The POM images of ascorbic acid, HSA, and a protein mixture (concentrations ranging from 50 μM to 400 μM) were captured (Fig. S1, ESI†), and GI calibration graphs were plotted, as shown in Fig. 8(b)–(d).

Results indicated that the R^2 values for 7CB-ascorbic acid (0.80759) and 7CB-HSA (0.41068) interactions were relatively lower, demonstrating limited specificity. In contrast, the 7CB-protein mixture containing human insulin yielded a significantly higher R^2 value of 0.92751, confirming its specificity for quantitative analysis. Table 1 illustrates how our biosensor differs from previously reported label-free biosensors.

3.2 Molecular docking study of 7CB-LC interacting with human insulin

Molecular docking can be considered as an optimisation problem, with the objective of determining the best-fit orientation of a ligand that binds to a specific protein. This technique entails altering the arrangement of both the protein and ligand to reach an ideal fit, similar to a ''hand-in-glove'' analogy rather than a ''lock-and-key'' paradigm.[20] In the case of 7CB-LC human insulin docking, 7CB is the ligand, which is flexible and human insulin is the rigid protein. Docking studies reveal the minimum binding energy site between the ligand and the protein, providing insights into their interaction and aiding in understanding the formation of specific textures observed under POM. Different types of molecular docking methods exist, such as geometric matching, stimulation-based, fragmentation, and conformational ensemble methods.[21] Among these methods, we follow the simulation-based method in which the protein and ligand are prepared using docking software. This method allows the ligand to find its minimum binding energy position at the protein active site through conformational changes. This kind of blind docking approach was used in our study for a flexible docking between 7CB and insulin. An in-depth detailed exploration of the docking mechanism is given in the ESI,† Section S1.

The human insulin structure obtained from the protein data bank consists of four chains: A, B, C, and D. Among the four chains, only chain B was considered for docking. By utilising a single chain, the docking process is streamlined, allowing for a more targeted examination of a particular protein structure without the added complexity of multiple chains. Blind docking was conducted using Auto Dock tool 1.5.7, which generated a data log (DLG) file containing all the details regarding the 7CB-insulin docking. Among the binding sites, the minimum binding energy site having an energy of -6.62 kcal mol^{-1} was considered for docking.

7CB-LC docked at the minimum binding energy site of insulin chain B is shown in Fig. 9(a). Numerous amino acid residues of human insulin were found around the 7CB ligand docking site (Fig. S2, ESI†), among which amino acid residues such as arginine (Arg) 22, cysteine (Cys) 19, phenylalanine (Phe) 25 and leucine (Leu) 15 of insulin were found to form interactions with 7CB at the minimum binding energy site as shown in Fig. 9(b). The amino acid residue arginine (Arg) 22 of human insulin formed a π-alkyl interaction with the first benzene ring of 7CB-LC, having a bond distance of 5.84 Å, as shown in Fig. 9(c). In addition to this, phenylalanine (Phe) 25 formed a π–π stacking having a bond distance of 4.61 Å with the second benzene ring of the 7CB ligand. The amino acid residue leucine (Leu) 15 formed an alkyl interaction having a bond distance of

Table 1 The performance of existing label-free biosensors for the detection of human insulin

Type of biosensor	Sample	Linear range	Detection limit	Ref.
Surface plasmon resonance (SPR) immuno-sensor (graphene field effect transistor)	Buffer solution and human serum	2.247–674.1 pmol L^{-1}	2.247 pmol L^{-1}	17
Electrochemical impedance spectroscopy	Buffer solution and human serum	5 pmol L^{-1}–50 nmol L^{-1}	1.2 pmol L^{-1}	18
LC-biosensor, (5CB-LC)	Buffer solution, human serum, and IGA3	0.1–1.0 nmol L^{-1}	0.1 nmol L^{-1}	9
Fluorescence-based biosensor	Chromene mimic receptors, buffer solution, and human serum	10 fmol L^{-1}–600 pmol L^{-1}	7.07 fmol L^{-1}	8
Interferometric reflectance spectroscopy (IRS)	Buffer solution, human islets, antibodies, and aptamers	11.235–112.35 nmol L^{-1}	2.247 pmol L^{-1}	19
LC-biosensor (7CB-LC)	Buffer solution and human serum	25 μM–500 μM	25 μmol L^{-1}	Reported here

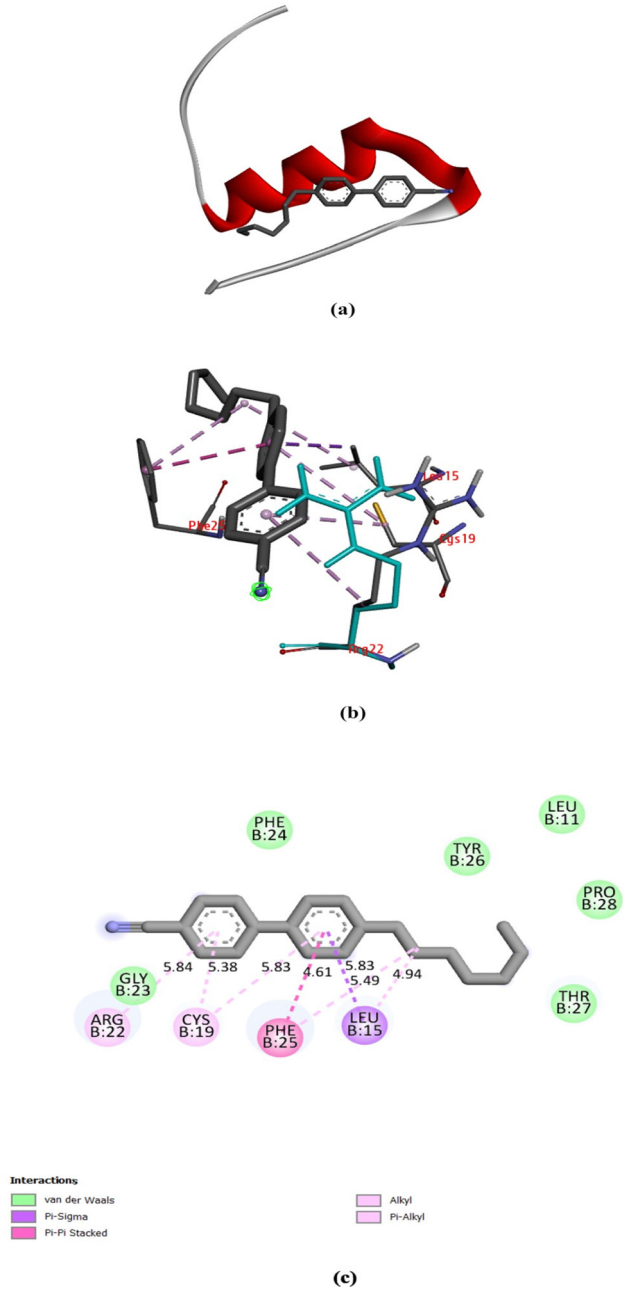

Fig. 9 (a) 7CB docked in the minimum binding energy site of human insulin, (b) amino acid residues surrounding 7CB-LC in the minimum binding energy site of human insulin visualised using a discovery studio visualiser (DSV), and (c) 2-dimensional representation of 7CB-LC docked with human insulin and all possible types of interactions made by the nearby amino acid residues.

4.94 Å with the C_{15} carbon atom of the 7CB ligand. Cysteine (Cys) 19 formed a π-alkyl interaction with both benzene rings of 7CB-LC, with a bond distance of 5.38 Å to the first benzene ring and 5.83 Å to the second benzene ring, as illustrated in Fig. 9(c).

All possible hydrophobic interactions made by the amino acid residues of human insulin surrounding the 7CB ligand are shown in Table 2 and Fig. 10(b). The amino acid reside phenylalanine (Phe) 25 forming a π-stacking interaction

Table 2 Hydrophobic interactions

Residue no	Residue type	Distance (Å)	Ligand atom	Protein atom
15B	Leucine (Leu)	3.34	329	141
22B	Arginine (Arg)	3.77	322	212
24B	Phenylalanine (Phe)	3.20	327	245
25B	Phenylalanine (Phe)	3.86	335	260
25B	Phenylalanine (Phe)	3.83	334	262
25B	Phenylalanine (Phe)	3.56	321	261
26B	Tyrosine (Tyr)	3.25	338	272

between human insulin and the 7CB ligand is shown in Table 3. Amino acid residues such as leucine (Leu) 15, arginine (Arg) 22, phenylalanine (Phe) 24,25 and tyrosine (Tyr) 26 were found to form hydrophobic interactions. In addition to this, van der Waals interactions were observed to be formed by amino acid residues such as phenylalanine (Phe) 24, leucine (Leu) 11, threonine (Thr) 27, tyrosine (Tyr) 26, proline (Pro) 28 and glycine (Gly) 23 as shown in Fig. 9(c).

In addition to hydrophobic interactions, properties such as aromaticity, H-bonds, solvent accessible area (SAS) and hydrophobicity were measured, as shown in Fig. 11. Aromatic interactions play a crucial role in influencing the binding affinity of ligands to proteins. They stabilise complexes, improve specificity, serve as binding hot spots, contribute energetically, and provide structural stability.[22] Aromatic amino acid residues such as phenylalanine (Phe), tyrosine (Tyr), tryptophan (Trp), and histidine (His) in the protein show aromatic properties towards the ligand in molecular docking. As shown in Fig. 11(a), amino acid residues phenylalanine (Phe) 15, leucine (Leu) 15 and arginine (Arg) 22 showed aromatic properties around the 7CB ligand. Among these, phenylalanine (Phe) 15 was found to form an edge-to-face interaction with the 7CB ligand. In this type of interaction, the edge of one aromatic ring of Phe (15) aligns with the face of another aromatic ring of the 7CB-ligand.[23] Other types of aromatic interactions in protein–ligand docking include π–π stacking, CH–π stacking and face-to-face π-stacking.[24]

Fig. 11(b) shows the H-bonds observed around the 7CB-insulin binding site. It can be seen that only the amino acid residue phenylalanine (Phe) 15 was found to be an H-bond donor in nature. Hydrogen bonds identified within ligand–protein binding sites are crucial in dictating the binding affinity and specificity of the interaction. They play a major role in the disruption of hydrogen bonds within the water molecules and the establishment of fresh hydrogen bonds between the protein and the ligand, thereby influencing the strength and selectivity of binding interactions.[25,26]

Solvent-accessible surface (SAS) is vital in protein–ligand interactions, measuring amino acid exposure to the surrounding environment, encompassing both the solvent and protein core. It aids in understanding how molecular interactions are influenced by the accessibility and arrangement of amino acids within the protein structure. The reduction in ligand SAS upon binding is a crucial indicator of ligand burial within the binding pocket. SAS calculations are important for elucidating protein–ligand interactions, enabling the identification of

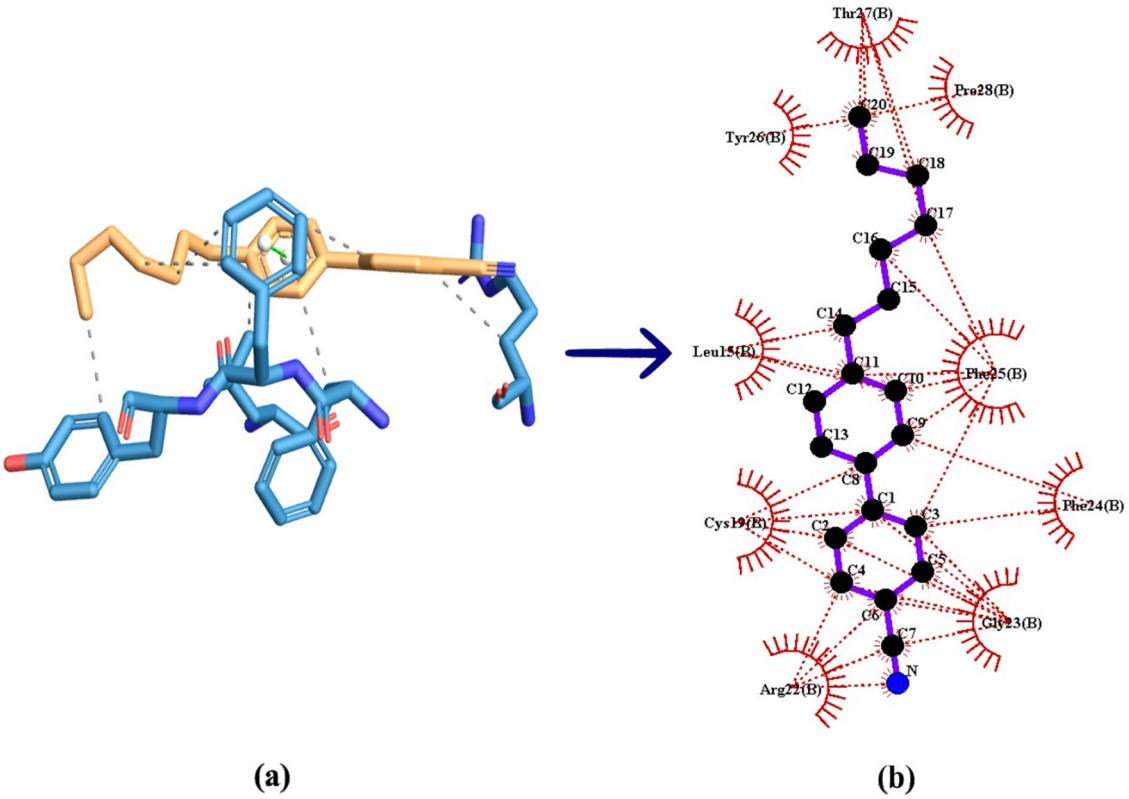

Fig. 10 (a) 3-Dimensional visualisation of the 7CB ligand docked at the minimum binding energy site of human insulin. (b) Hydrophobic interaction made by human insulin docked with 7CB visualised using Ligplot + V 2.2.

Table 3 π-Stacking

Residue no.	Residue type	Distance (Å)	Angle	Stacking type	Ligand atoms
25B	Phenylalanine (Phe)	4.48	21.94	P	326, 327, 328, 329, 330, 331

binding sites, estimation of binding affinities, and advancement of novel sampling algorithms for molecular design.[27,28] In the case of 7CB-insulin docking, amino acid residues such as phenylalanine (Phe) 15, leucine (Leu) 15 and arginine (Arg) 22 showed SAS properties, as shown in Fig. 11(c).

Hydrophobic interactions between the hydrophobic regions of proteins and ligands enhance the stability and specificity of the binding complex in molecular docking. The hydrophobic effect, stemming from the behaviour of hydrophobic molecules to cluster in water-based surroundings, is crucial in governing protein–ligand interactions.[29,30] In the case of 7CB-insulin docking, amino acid residues such as phenylalanine (Phe) 15 and leucine (Leu) 15 were found to be hydrophobic and arginine (Arg) 22 hydrophilic, as shown in Fig. 11(d).

Molecular docking complements the POM studies since it provides detailed insights into the molecular-level interaction between proteins and ligands. Docking offers insights into ligand binding sites, identifies the interactions occurring at these sites, and facilitates the visualisation of ligand–protein binding on a molecular scale. It helps identify the change in the position of 7CB tail ends at which the amino acid residues of the insulin interact. Raman studies are conducted to learn more about the segmental mobility of different parts of LC and changes happening in the core and terminal changes due to insulin interactions. Raman studies provide structural information regarding conformational changes and changes in vibrational modes that 7CB-LC undergoes on docking with different concentrations of human insulin.

3.3 Investigation of the 7CB–human insulin complex using Raman spectroscopy

Conformational and structural alterations in the vibrational modes of 7CB-LC induced by various concentrations of human insulin are investigated using Raman spectroscopy. The analysis includes examining shifts in the peak position, changes in the line width, and variations in intensity. The peak position in the Raman spectrum corresponds to the specific vibrational mode of the molecule. It gives information regarding the energy linked with each vibrational mode. The frequency of the Raman peak is directly related to the energy of the vibrational mode. This relationship between the frequency of the Raman peak and the energy of vibrational mode in the Raman

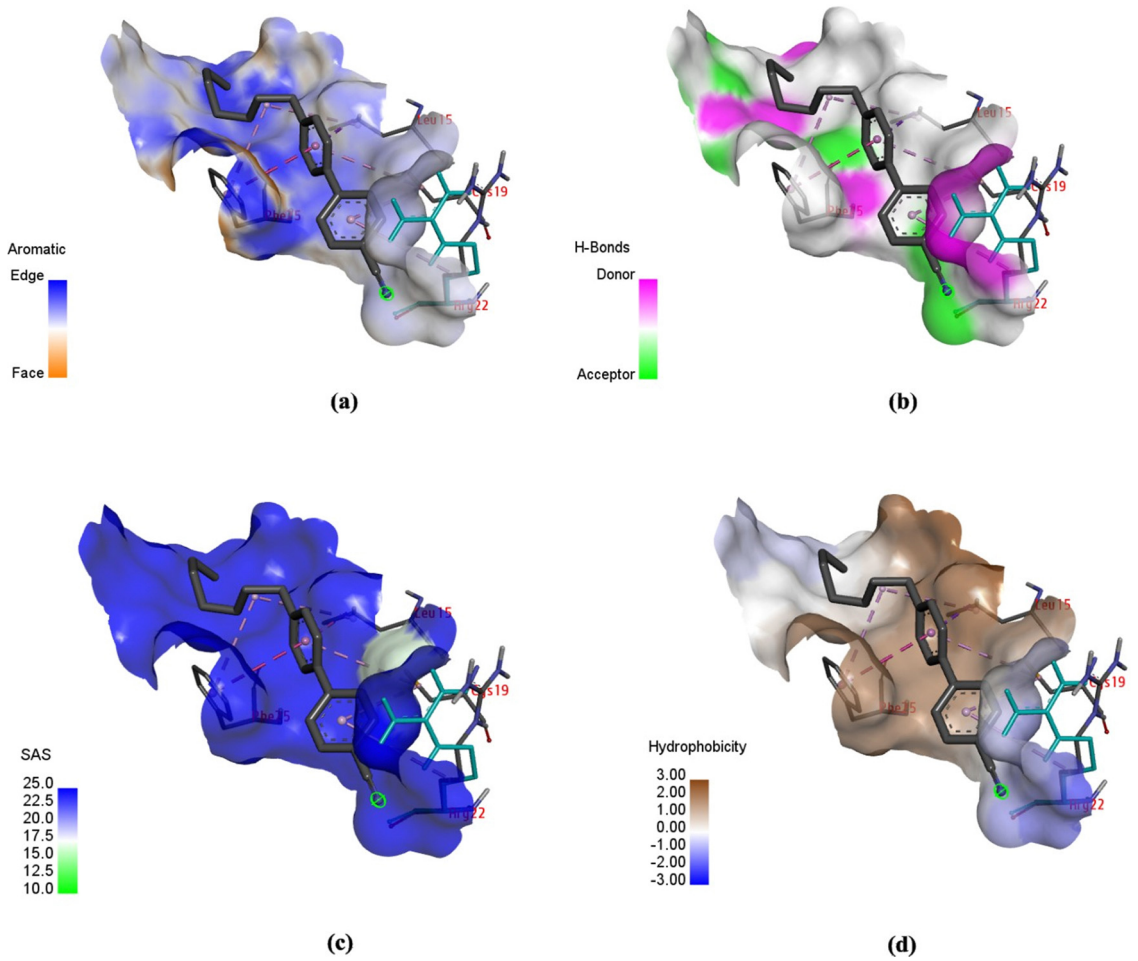

Fig. 11 Schematic of (a) aromaticity, (b) H-bonds, (c) solvent-accessible area (SAS), and (d) hydrophobicity exhibited by the human insulin (chain B) docked with 7CB-LC (visualised using DSV).

spectra helps identify vibrations in specific functional groups. The peak position acts as a fingerprint for each sample.[31]

Line width in the Raman spectra provides information about a change in the lifetime, energy distribution and broadening of vibrational modes with respect to a change in the concentration of the sample. Integrated intensity in the Raman spectra helps measure the amount of light scattered by the sample at a specific frequency of vibrations. It measures the overall magnitude of a specific vibrational mode in the Raman spectra.[32] Measuring integrated intensity provides insights into the change in structural characteristics that the sample undergoes with respect to the change in the concentration of the sample.[33]

The Raman spectra of pure 7CB-LC show that major peaks were observed at wavelengths 1180 cm^{-1}, 1287 cm^{-1}, 1525 cm^{-1}, 1608 cm^{-1}, 2223 cm^{-1} and 2848 cm^{-1}, as shown in Fig. 12(a). Changes in the Raman spectra of 7CB-LC on adding different concentrations of insulin, such as 25 μM, 50 μM, 100 μM, 200 μM, 300 μM, 400 μM, and 500 μM, are shown in Fig. 12(b). For a detailed analysis, the spectral regions were segmented into three intervals: a vibrational region of 1160 cm^{-1} to 1320 cm^{-1}, a vibrational region of 1580 cm^{-1} to 2235 cm^{-1}, and a vibrational region of 2853 cm^{-1} to 3000 cm^{-1}. A detailed mechanism exploration of Fig. 12 is given in Section S2 in the ESI.†

3.3.1. Study of Raman parameters in the spectral region 1160–1320 cm^{-1}. Two prominent peaks were observed in the spectrum of 7CB-LC between 1160 and 1320 cm^{-1}. The first peak appears at 1180 cm^{-1}, and the second peak was observed at 1288 cm^{-1}, as illustrated in Fig. 13(a). These peaks within the 1160 to 1320 cm^{-1} range are attributed to the in-plane deformations of C–H bonds within the aromatic rings.[34] 7CB-LC, when interacting with insulin, causes minor shifts in these peaks, as shown in Table 4. This shift in the peak position (PP) of 1180 cm^{-1} was due to the C–H in-plane deformations in the presence of phenylalanine (Phe) amino acid in human insulin. The peak position (PP) shift of 1287 cm^{-1} was observed due to the influence of amide III bands present in insulin.[35]

For lower concentrations ranging from 25 μM to 100 μM, the shift in PP was towards a higher frequency. However, for concentrations between 200 μM and 500 μM, the PP shift moved towards a lower frequency, as illustrated in Fig. 13(a). This shift in PP happens because the molecule's vibrational behaviour is affected when the sample's concentration changes. This difference in vibrational behaviour changes the

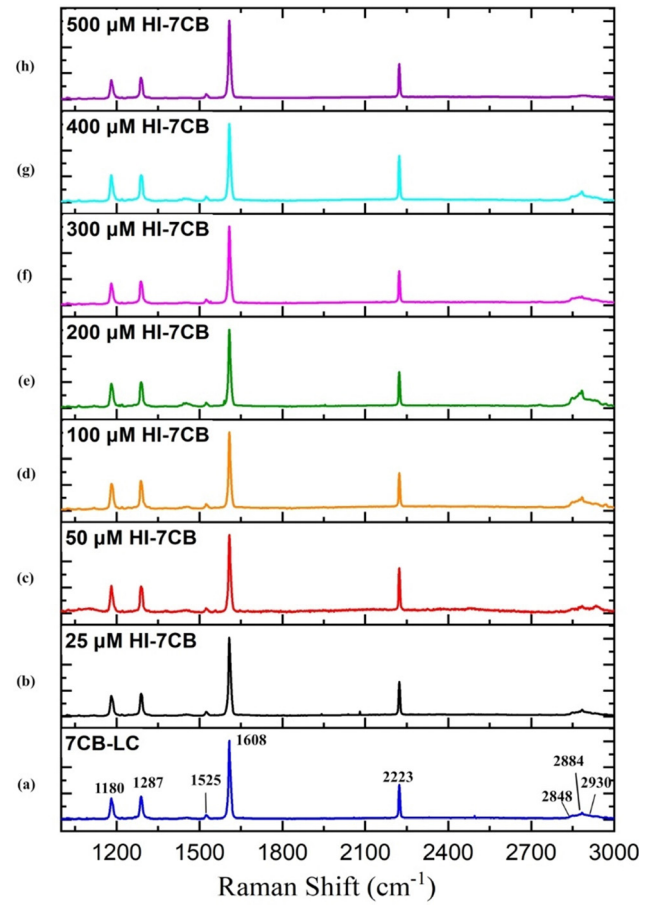

Fig. 12 Raman spectra of 7CB liquid crystal and its corresponding peaks in the range between 1000 cm^{-1} and 3000 cm^{-1} and Raman spectra obtained for the 7CB–insulin complex for concentrations such as (a) 7CB-LC, (b) 25 μM, (c) 50 μM, (d) 100 μM, (e) 200 μM, (f) 300 μM, (g) 400 μM, and (h) 500 μM.

interaction between the LC and insulin, leading to a shift in PP. A variation in the chemical environment and molecular interactions can cause a change in vibrational energy, which leads to a shift in PP.

The linewidth (LW) analysis reveals a gradual decrease in the LW for the 1180 cm^{-1} peak till 400 μM concentration of HI, and beyond which it increases. Similarly, for the 1287 cm^{-1} peak, a decrease in the LW was observed until a concentration of 100 μM, beyond which it remained constant, as shown in Fig. 14(b). A decrease in the LW indicated that the sample has a well-defined isolated vibrational mode. The increase in the LW indicated the broadening of the LW due to the change in molecular interactions and vibrational energy resulting from different sample concentrations.

Integrated intensity (II) analyses of the peaks in this range reveal a consistent trend. Since there were changes in the background as we vary concentrations, the intensities were normalised to understand the relative intensities of peaks at different concentrations. The normalised intensities were treated as percentage contributions and were termed integrated intensities. The II initially decreases up to 50 μM, then increases to 200 μM concentration of HI. Subsequently, there is another decrease until 400 μM, followed by an increase till 500 μM. These trends are represented in Fig. 14(c).

3.3.2. Study of Raman parameters in the spectral region 1580–2235 cm^{-1}. Three prominent peaks were observed in the spectral range of 1580–2235 cm^{-1} of 7CB-LC. The first and second peaks observed at 1525 cm^{-1} and 1608 cm^{-1}, as shown in Fig. 13(b) and (c), are due to the stretching of C–C in the aromatic rings.[34] The third peak observed at 2223 cm^{-1}, as shown in Fig. 13(d), is assigned to the cyano (C≡N) stretching observed in 7CB-LC. 7CB-LC, when interacting with insulin, showed a shift in these peaks, as shown in Table 4.

The alteration in the PP at 1525 cm^{-1} is attributed to the presence of amide II bands, specifically involving C–C stretching within insulin. The change in the PP at 1608 cm^{-1} corresponds to the stretching of aromatic ring (C–C) bonds, indicative of the phenylalanine (Phe) amino acid in insulin. Additionally, the shift in the PP at 2223 cm^{-1} is due to the stretching of the cyano (C≡N) group in the presence of insulin. A shift in the PP towards a higher frequency range was observed up to 100 μM concentrations of HI, beyond which the PP shifts towards a lower frequency, as illustrated in Fig. 13(b)–(d) and Table 4. LW analysis of 1525 cm^{-1} shows an increase in the LW till 100 μM, beyond which it decreases. In the LW analysis of 1608 cm^{-1}, a decline in the LW is noted up to a concentration of 300 μM. Beyond this concentration, up to 400 μM, the LW increased, as depicted in Fig. 14(b). Subsequently, from 400 μM to 500 μM concentration, the LW decreased once more. LW analysis of 2223 cm^{-1} shows an increase in the LW till 100 μM, beyond which it decreases till 300 μM and increases afterwards. The II analysis of the three peaks within this range demonstrates a consistent pattern similar to what was observed in the vibrational region spanning 1160 to 1320 cm^{-1} and is illustrated in Fig. 14(c). The consistent pattern observed in the range from 1160 to 2223 cm^{-1} can be attributed to the composition of the 7CB-LC core, as indicated in Table 4. This core portion of 7CB-LC exhibits higher organisation levels than the terminal tail. When interacting with varying insulin concentrations, the core undergoes reorientation to achieve a more favourable configuration.

3.3.3. Study of Raman parameters in the spectral region 2853–3000 cm^{-1}. Three prominent peaks were observed in the region 2853–3000 cm^{-1}, as shown in Fig. 13(e). The two initial peaks detected at 2848 cm^{-1} and 2884 cm^{-1} arise from the symmetric stretching of C–H bonds within the aliphatic chains, specifically representing the CH_2 groups. The third peak at 2930 cm^{-1} corresponds to the asymmetric stretching of C–H bonds within aliphatic chains, associated explicitly with CH_3 groups. A shift in these peaks when interacting with insulin is observed due to the presence of phenylalanine (Phe) in insulin.

For the case of 2848 cm^{-1}, a rise in the peak position (PP) and linewidth (LW) was observed until reaching 100 μM, after which they decreased. Subsequently, from 300 μM to 400 μM, there was a noticeable increase in both the PP and LW, followed by a decrease thereafter, as depicted in Fig. 13(e) and 14(a). In the case of 2884 cm^{-1}, an increase in the PP is observed until

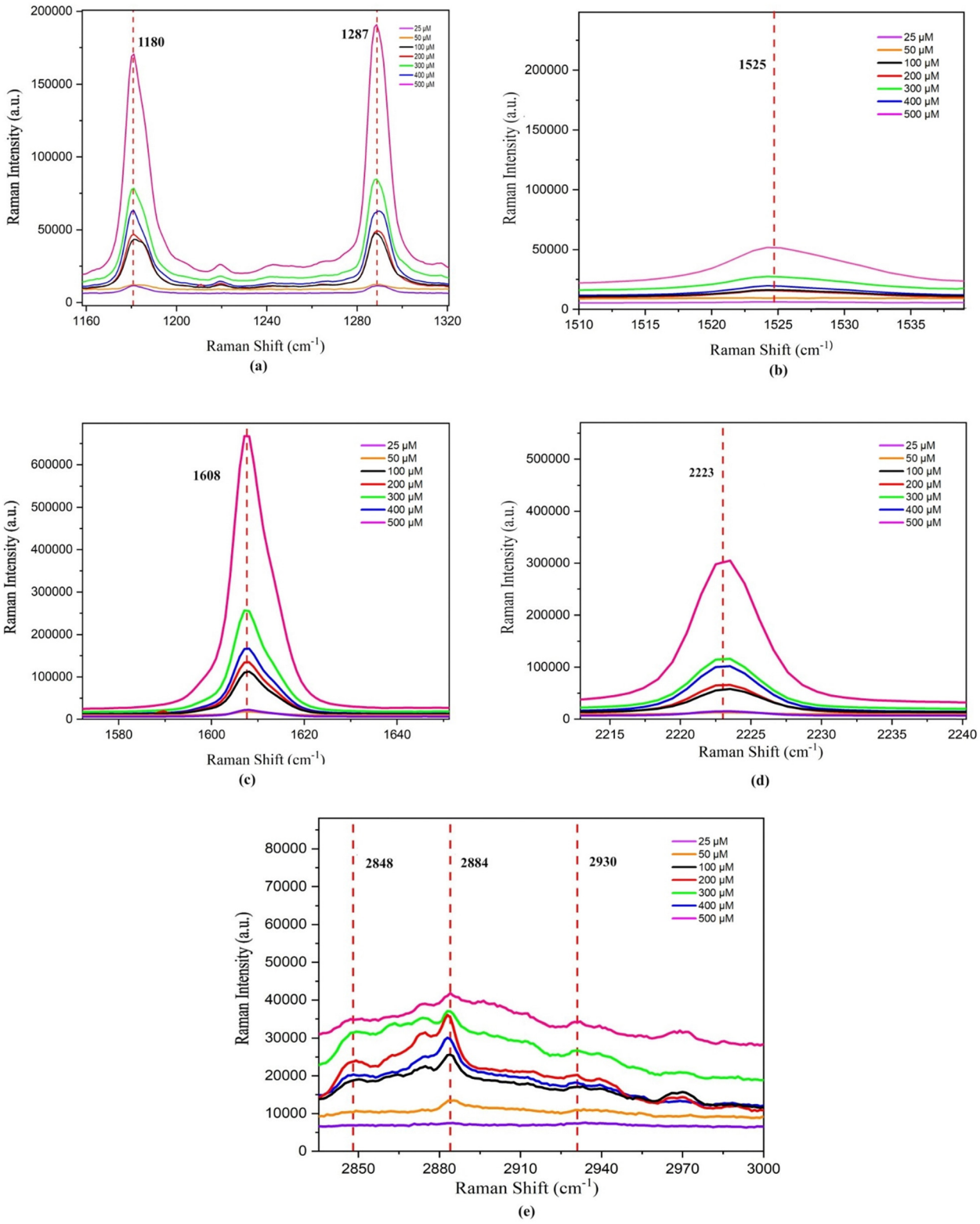

Fig. 13 Change in the peak position for different concentrations of the 7CB–insulin complex observed for the regions: (a) vibrational region 1160–1320 cm^{-1}, (b) vibrational region 1510–1540 cm^{-1}, (c) vibrational region 1580–1650 cm^{-1}, (d) vibrational region 2215–2235 cm^{-1} and (e) vibrational region 2853–3000 cm^{-1}.

it reaches 50 μM. Beyond this concentration, the PP shifts towards lower frequencies. However, beyond 400 μM, there is a shift towards higher frequencies in the PP, as illustrated in Fig. 13(e). Regarding the peak at 2884 cm^{-1}, the LW and II both

Table 4 Interpretation of Raman vibrational bands observed in the Raman spectra of the 7CB-LC and the 7CB–insulin combinations

Pure 7CB-LC ($\Delta\nu$) cm^{-1}	Band assignment for pure 7CB-LC	7CB-LC bonded with insulin concentrations (25 μM, 50 μM, 100 μM, 200 μM, 300 μM, 400 μM, and 500 μM) ($\Delta\nu$) cm^{-1}	Band assignment for the 7CB–human insulin complex
1180	Aromatic C–H in-plane deformation	1180.19, 1180.13, 1180.24, 1179.82, 1179.95, 1179.94, and 1179.97	Aromatic C–H in-plane deformation in the presence of phenylalanine (Phe)
1287	ν(C–C) of biphenyl	1287.20, 1286.59, 1286.95, 1286.96, 1286.74, 1286.85, and 1286.94	Amide III bands (involves significant C–N stretching, N–H bending and C–C stretching)
1525	ν(C–C) of aromatic rings	1525.51, 1525.58, 1525.54, 1525.40, 1525.31, 1525.39, and 1525.39	Amide II bands (involves significant C–N stretching, N–H bending, and C–C stretching)
1608	ν(C–C) of aromatic rings	1608.46, 1608.43, 1608.43, 1608.29, 1608.18, 1608.34, and 1608.26	ν(C–C) of aromatic rings in the presence of phenylalanine (Phe)
2223	ν(C$\equiv$N)	2223.25, 2223.44, 2223.42, 2223.23, 2223.15, 2223.18, and 2223.20	ν(C$\equiv$N)
2848	ν-s(C–H) in aliphatic chains	2848.71, 2848.62, 2864.51, 2848.83, 2848.84, 2867.62, and 2848.20	ν-s(C–H) in aliphatic chains (CH_2) along with phenylalanine (Phe) in insulin
2884	ν-s(C–H) in aliphatic chains	2882.57, 2885.49, 2883.69, 2877.86, 2876.92, 2882.89, and 2886.65	ν-s(C–H) in aliphatic chains (CH_2) along with phenylalanine (Phe) in insulin
2930	ν-as(C–H) in aliphatic chains	2936.35, 2940.58, 2936.61, 2930.57, 2922.84, 2951.58, and 2946.01	ν-as(C–H) in aliphatic chains (CH_3) along with phenylalanine (Phe) in insulin

ν – stretching, ν-s – symmetric stretching, and ν-as – asymmetric stretching.

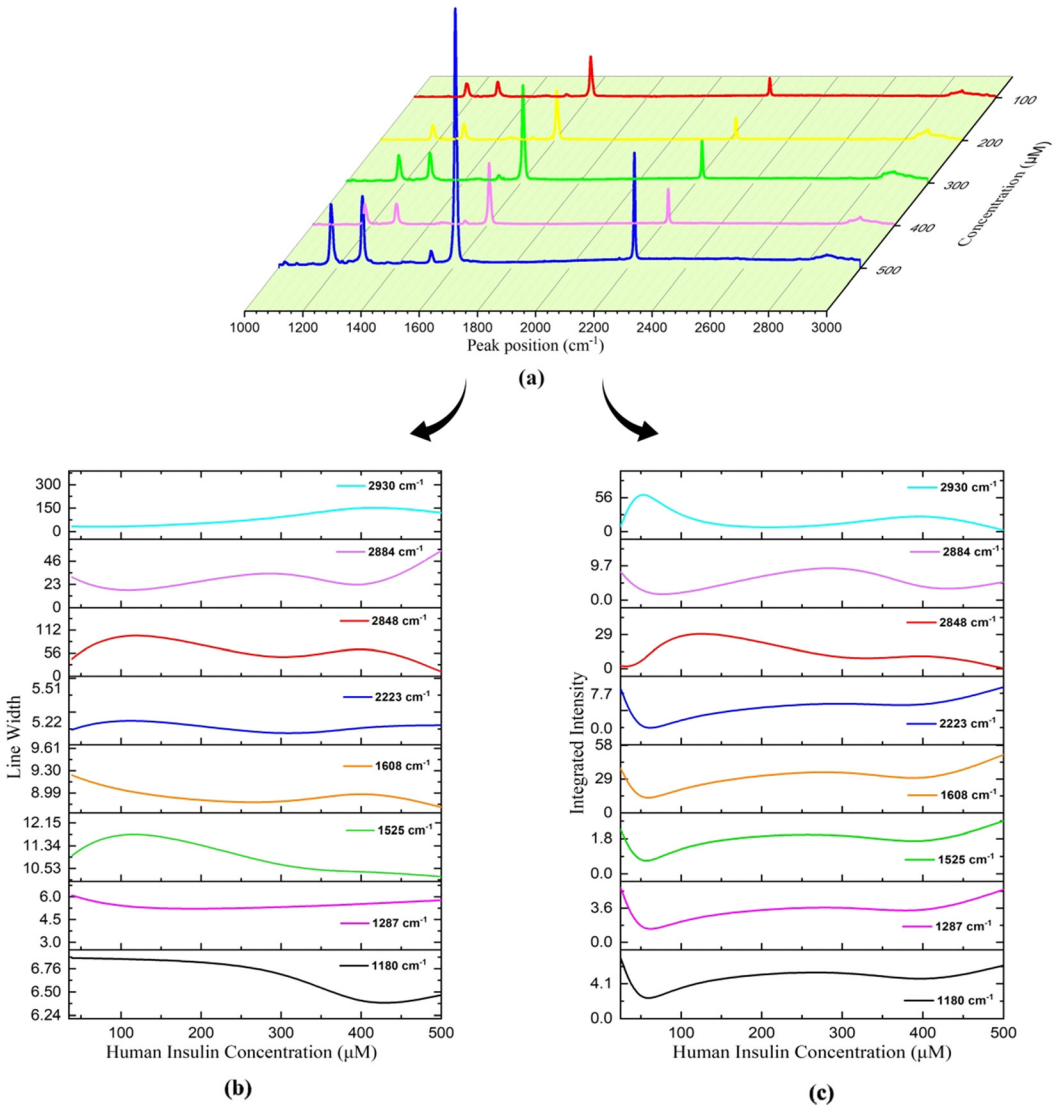

Fig. 14 Variation in Raman parameters for different concentrations of the 7CB–insulin complex: (a) peak position, (b) line width, and (c) integrated intensity.

show a similar trend, as shown in Fig. 14(b) and (c). A decrease in the LW until 100 μM was observed, after which it increased. Subsequently, it starts decreasing again from 300 μM and increases above 400 μM. A trend similar to the LW was observed in the case of II, as shown in Fig. 14(c).

The PP analysis of the peak 2884 cm^{-1} shows an increase in the shift to a higher frequency range till 50 μM, beyond which it decreases and then increases on reaching 400 μM concentration of HI. A trend opposite to 2848 cm^{-1} was observed in the case of the LW and II analysis of 2884 cm^{-1}, as shown in Fig. 14(b) and (c). A similar trend in frequency shift was observed in the PP analysis of the peak at 2930 cm^{-1}, as shown in Table 4. The peak at 2930 cm^{-1} occurs due to the asymmetric stretching of (C–H) in aliphatic chains (CH_3) along with phenylalanine (Phe) in insulin. The observed trends in the II across this region can be explained by the composition of the aliphatic chains within the 7CB-LC, as detailed in Table 4. These terminal tails undergo reconfiguration in response to interactions with varying concentrations of human insulin, thus demonstrating the observed patterns. The LW increases gradually till 400 μM and decreases beyond it, as shown in Fig. 14(b). The II analysis shows that II increases till 50 μM concentration of HI and beyond which it decreases till 200 μM. An increase in II was observed till 400 μM, which decreases upon reaching a higher concentration, as shown in Fig. 14(c). Raman studies reveal that the aliphatic chains of 7CB-LC are highly sensitive to human insulin concentrations. This is demonstrated by irregular changes in the integrated intensity data beyond the 2853 cm^{-1} range.

4. Conclusion

In this study, a novel prototype for label-free detection of human insulin detection using a 7CB-liquid crystal is developed. 7CB, when interacting with human insulin on a DMOAP-coated glass substrate, showed a distinct director orientation for different concentrations of human insulin. Concentrations ranging from 25 μM to 500 μM were studied under a polarising optical microscope, and textures such as radial, twisted-radial, pre-radial and bipolar were observed. A selectivity study conducted using Image J analysis showed a positive correlation graph between the average grey scale index and the insulin concentration, having an R^2 value of 0.97279. Molecular docking and Raman spectroscopy studies conducted for different concentrations of human insulin interacting with 7CB-LC showed that the aliphatic chains and the biphenyl rings of 7CB-LC undergo symmetric and asymmetric stretching in the presence of amino acid residues such as phenylalanine (Phe) present in human insulin. A change in the peak position, line width and integrated intensity in the 7CB-LC spectra was observed due to the interaction of human insulin. Raman studies indicate that the aliphatic chains of 7CB-LC exhibit greater sensitivity to human insulin concentrations, as evidenced by the irregular changes in the integrated intensity data beyond the 2853 cm^{-1} range. A detection limit of 25 μM was observed for the proposed prototype, which is a limitation since it does not meet the required detection limit. This study provides a unique way of utilising 7CB-LC for human insulin detection using both time and temperature sensing methods. It was observed that among all the LC sensors existing for human insulin detection, 7CB-LC shows better stability and visualisation in terms of the label-free detection method since it shows significant LC–human insulin interaction textures with respect to both time and temperature. However, efforts are ongoing to enhance the biosensor to meet essential detection criteria, aiming for achieving improved performance in upcoming experiments.

Data availability

The data supporting the findings of this study are available within the article and its ESI.† Additional datasets generated and analysed during the current study are available from the corresponding author upon reasonable request. Any other data related to this study can be obtained from the authors upon request, ensuring compliance with data protection and confidentiality agreements.

Conflicts of interest

There are no conflicts to declare.

Acknowledgements

The authors would like to thank the DST-FIST Project. [File no SR/FST/PS-I/2019/74] for the financial assistance and the Department of Physics, National Institute of Technology Meghalaya, for the instrumentation facilities for polarising optical microscopy and Raman Spectroscopy.

References

1 S. Chandrasekhar, *Liquid Crystals*, 1992.
2 V. K. G. Abbot, Optical Amplification of Ligand-Receptor, *Science*, 1998, **279**, 2077–2080.
3 M. S. Rahman, K. S. Hossain, S. Das, S. Kundu, E. O. Adegoke, M. A. Rahman, M. A. Hannan, M. J. Uddin and M. G. Pang, *Int. J. Mol. Sci.*, 2021, 22.
4 G. Wilcox, *Insulin and Insulin Resistance*, 2005, vol. 26.
5 S. Y. Park, J. F. Gautier and S. Chon, *Diabetes Metab. J.*, 2021, **45**, 641–654.
6 W. Yoshida, E. Mochizuki, M. Takase, H. Hasegawa, Y. Morita, H. Yamazaki, K. Sode and K. Ikebukuro, Selection of DNA aptamers against insulin and construction of an aptameric enzyme subunit for insulin sensing, *Biosens. Bioelectron.*, 2009, **24**, 1116–1120.
7 A. Garcia Cruz, I. Haq, T. Cowen, S. Di Masi, S. Trivedi, K. Alanazi, E. Piletska, A. Mujahid and S. A. Piletsky, Design and fabrication of a smart sensor using in silico epitope mapping and electro-responsive imprinted polymer nanoparticles for determination of insulin levels in human plasma, *Biosens. Bioelectron.*, 2020, **169**, 112536.

8 K. L. Servarayan, E. Sundaram, A. Manna and V. Sivasamy, Label free optical biosensor for insulin using naturally existing chromene mimic synthesized receptors: A green approach, *Anal. Chim. Acta*, 2023, 1239.
9 J. Chen, Z. Liu, R. Yang, M. Liu, H. Feng, N. Li, M. Jin, M. Zhang and L. Shui, A liquid crystal-based biosensor for detection of insulin driven by conformational change of an aptamer at aqueous-liquid crystal interface, *J. Colloid Interface Sci.*, 2022, **628**, 215–222.
10 G. M. Morris and M. Lim-Wilby, Molecular Docking, *Methods Mol. Biol.*, 2008, **443**, 365–382.
11 L. F. Gonçalves Dias, S. Stamboroski, M. Noeske, D. Salz, K. Rischka, R. Pereira, M. Do Carmo Mainardi, M. H. Cardoso, M. Wiesing, E. S. Bronze-Uhle, R. B. Esteves Lins and P. N. Lisboa-Filho, New details of assembling bioactive films from dispersions of amphiphilic molecules on titania surfaces, *RSC Adv.*, 2020, **10**, 39854–39869.
12 M. Škarabot, E. Osmanagič and I. Muševič, Surface anchoring of nematic liquid crystal 8OCB on a DMOAP-silanated glass surface, *Liq. Cryst.*, 2006, **33**, 581–585.
13 O. O. Prishchepa, V. Y. Zyryanov, A. P. Gardymova and V. F. Shabanov, Optical textures and orientational structures of nematic and cholesteric droplets with heterogeneous boundary conditions, *Mol. Cryst. Liq. Cryst.*, 2008, **489**, 84/[410]–93/[419].
14 M. Cieplak, R. Węgłowski, Z. Iskierko, D. Węgłowska, P. S. Sharma, K. R. Noworyta, F. D'souza and W. Kutner, *Sensors*, 2020, **20**, 1–12.
15 Y. Y. Luk, M. L. Tingey, D. J. Hall, B. A. Israel, C. J. Murphy, P. J. Bertics and N. L. Abbott, Using liquid crystals to amplify protein-receptor interactions: Design of surfaces with nanometer-scale topography that present histidine-tagged protein receptors, *Langmuir*, 2003, **19**, 1671–1680.
16 M. H. Pourasl, A. Vahedi, H. Tajalli, B. Khalilzadeh and F. Bayat, Liquid crystal-assisted optical biosensor for early-stage diagnosis of mammary glands using HER-2, *Sci. Rep.*, 2023, **13**, 6847.
17 Z. Hao, Y. Zhu, X. Wang, P. G. Rotti, C. Dimarco, S. R. Tyler, X. Zhao, J. F. Engelhardt, J. Hone and Q. Lin, Real-Time Monitoring of Insulin Using a Graphene Field-Effect Transistor Aptameric Nanosensor, *ACS Appl. Mater. Interfaces*, 2017, **9**, 27504–27511.
18 M. Xu, X. Luo and J. J. Davis, The label free picomolar detection of insulin in blood serum, *Biosens. Bioelectron.*, 2013, **39**, 21–25.
19 R. Chhasatia, M. J. Sweetman, F. J. Harding, M. Waibel, T. Kay, H. Thomas, T. Loudovaris and N. H. Voelcker, Non-invasive, *in vitro* analysis of islet insulin production enabled by an optical porous silicon biosensor, *Biosens. Bioelectron.*, 2017, **91**, 515–522.
20 W. Jorgensen, Rusting of the lock and key model for protein-ligand binding, *Science*, 1991, **254**, 954–955.
21 X.-Y. Meng, H.-X. Zhang, M. Mezei and M. Cui, Molecular Docking: A powerful approach for structure-based drug discovery, *Curr. Comput.-Aided Drug Des.*, 2011, **7**(2), 146–157.
22 M. Brylinski, Aromatic interactions at the ligand–protein interface: Implications for the development of docking scoring functions, *Chem. Biol. Drug Des.*, 2018, **91**, 380–390.
23 G. Ercolani and P. Mencarelli, Role of face-to-face and edge-to-face aromatic interactions in the inclusion complexation of cyclobis(paraquat-p-phenylene): A theoretical study, *J. Org. Chem.*, 2003, **68**, 6470–6473.
24 E. Lanzarotti, L. A. Defelipe, M. A. Marti and A. G. Turjanski, Aromatic clusters in protein–protein and protein–drug complexes, *J. Cheminf.*, 2022, **7**, 100079.
25 E. Nittinger, T. Inhester, S. Bietz, A. Meyder, K. T. Schomburg, G. Lange, R. Klein and M. Rarey, Large-Scale Analysis of Hydrogen Bond Interaction Patterns in Protein-Ligand Interfaces, *J. Med. Chem.*, 2017, **60**, 4245–4257.
26 H. Zhao and D. Huang, Hydrogen bonding penalty upon ligand binding, *PLoS One*, 2011, **6**(6), 19923.
27 K. Konstantinidis, I. Karakasiliotis, K. Anagnostopoulos and G. C. Boulougouris, On the estimation of the molecular inaccessible volume and the molecular accessible surface of a ligand in protein-ligand systems, *Mol. Syst. Des. Eng.*, 2021, **6**, 946–963.
28 E. Durham, B. Dorr, N. Woetzel, R. Staritzbichler and J. Meiler, Solvent accessible surface area approximations for rapid and accurate protein structure prediction, *J. Mol. Model.*, 2009, **15**, 1093–1108.
29 J. Li, C. Hou, M. Wang, C. Liao, S. Guo, L. Shi, X. Ma, H. Zhang, S. Jiang, B. Zheng, L. Ye, L. Yang and X. He, A Hydrophobic-Interaction-Based Mechanism Triggers Docking between the SARS-CoV-2 Spike and Angiotensin-Converting Enzyme 2, *Glob. Chall.*, 2020, **4**(12), 2000067.
30 Y. Cao and L. Li, Improved protein-ligand binding affinity prediction by using a curvature-dependent surface-area model, *Bioinformatics*, 2014, **30**, 1674–1680.
31 Y. C. Cho and S. Il Ahn, Fabricating a Raman spectrometer using an optical pickup unit and pulsed power, *Sci. Rep.*, 2020, **13**, 6847.
32 S. Maeda and C. H. Haruhiko Kataoka, *Effects of laser linewidth on the coherent Anti–Stokes Raman spectroscopy spectral profile*, 1982, vol. 36.
33 J. C. Evans and H. J. Bernstein, INTENSITY IN THE RAMAN EFFECT: V. THE EFFECT OF INTERMOLECULAR INTERACTION ON THE RAMAN SPECTRUM OF CARBON DISULPHIDE, *Can. J. Chem.*, 1956, **34**(8), 1127–1133.
34 D. Tuschel, Exploring Resonance Raman Spectroscopy, *Spectroscopy*, 2018, **33**, 12–19.
35 D. Kurouski, M. Sorci, T. Postiglione, G. Belfort and I. K. Lednev, Detection and structural characterization of insulin prefibrilar oligomers using surface enhanced Raman spectroscopy, *Biotechnol. Prog.*, 2014, **30**, 488–495.

